

# Targeted migration of pherophorin-S indicates extensive extracellular matrix dynamics in *Volvox carteri*

Benjamin von der Heyde  and Armin Hallmann\* 

Department of Cellular and Developmental Biology of Plants, University of Bielefeld, Universitätsstr. 25, Bielefeld 33615, Germany

Received 6 February 2020; revised 12 June 2020; accepted 17 June 2020; published online 30 June 2020.

\*For correspondence (e-mail armin.hallmann@gmx.de).

## SUMMARY

Hydroxyproline-rich glycoproteins (HRGPs) constitute a major group of proteins of the extracellular matrix (ECM). The multicellular green alga *Volvox carteri* is a suitable model organism in which to study the evolutionary transition to multicellularity, including the basic principles and characteristics of an ECM. In *Volvox*, the ECM is dominated by a single HRGP family: the pherophorins. Our inventory amounts to 117 pherophorin-related genes in *V. carteri*. We focused on a pherophorin with an unexpected characteristic: pherophorin-S is a soluble, non-cross-linked ECM protein. Using transformants expressing a YFP-tagged pherophorin-S we observed the synthesis and secretion of pherophorin-S by somatic cells *in vivo*, and we then traced the protein during its conspicuous migration to the ECM around prehatching juveniles and its localized concentration there. Our results provide insights into how an ECM zone surrounding the progeny is remotely affected by distantly located parental somatic cells. In view of the properties and migration of pherophorin-S, we conclude that pherophorin-S is likely to act as an ECM plasticizer to allow for dynamic ECM remodeling.

**Keywords:** extracellular matrix (ECM), *Volvox carteri*, pherophorins, sex-inducer protein, green algae, confocal laser scanning microscopy, multicellularity, *Chlamydomonas reinhardtii*.

## INTRODUCTION

One of the most important innovations in the history of life has been the evolutionary transition from unicellular to multicellular species, with the division of labor between germline and somatic cells. To investigate this evolutionary transition, the spheroidal green alga *Volvox carteri* and its close relatives have long been seen as suitable model organisms. These volvocine algae diverged relatively recently from unicellular relatives, and extant species display a range of organizational complexity, from unicellular and colonial genera to multicellular genera with full germ–soma division (Kirk, 1998, 2001, 2003, 2005; Hallmann, 2003; Nozaki, 2003; Schmitt, 2003; Kirk and Kirk, 2004; Michod *et al.*, 2006). During the evolution of multicellularity, a key step was the development of a complex, multifunctional extracellular matrix (ECM) out of the simple cell wall of a unicellular ancestor. In volvocine algae, ECM development is supposed to be one of only five essential steps on the path to differentiated multicellularity (Kirk, 2005). The surprisingly elaborated ECM of *V. carteri* consists of many region-specific and anatomically distinct structures arranged in a defined spatial pattern (Kirk *et al.*, 1986; Hallmann, 2003) (Figure 1). These ECM structures are supposed

to be modified under physiological, metabolic or developmental control. The architecture, chemical properties and the building blocks of the *Volvox* ECM, and its potential influence on developmental events, therefore, have been the subject of a number of studies (Sumper and Hallmann, 1998; Hallmann, 2003). The cell walls or ECMs of both unicellular volvocine algae, like *Chlamydomonas*, and multicellular volvocine algae, like *Volvox*, are known to be assembled mainly from hydroxyproline-rich glycoproteins (HRGPs), which not only dominate the ECM composition of green algae but also represent a main constituent of the ECMs of embryophytic land plants (Miller *et al.*, 1972; Sommer-Knudsen *et al.*, 1998; Sumper and Hallmann, 1998; Hallmann, 2003; Showalter and Basu, 2016).

The first ECM glycoprotein of *Volvox* to be identified and characterized was SSG185 (Ertl *et al.*, 1989). This sulfated HRGP was suggested to be one of the main components of CZ3 (Figure 1). A few years later, pherophorins I and II were characterized and roughly assigned to the CZ (Sumper *et al.*, 1993); a special feature of pherophorin II was its synthesis in response to the sex-inducer protein. The identification of further pherophorins, pherophorin III (Godl *et al.*, 1995), pherophorin-DZ1 (Ender *et al.*, 2002),

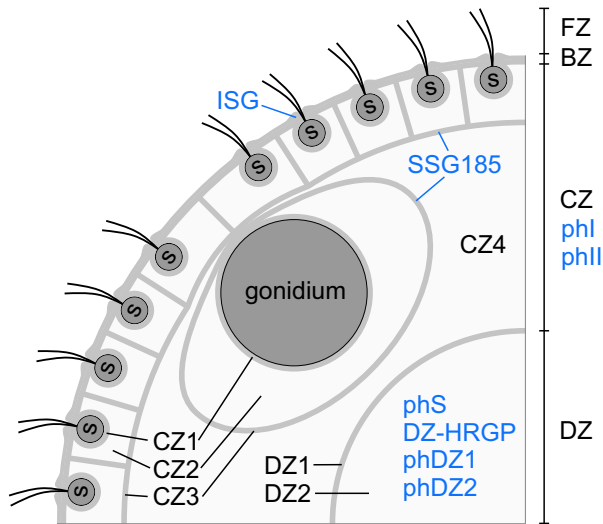


**Figure 1.** Schematic cross section of a *Volvox carteri* spheroid with the localization of known extracellular matrix (ECM) glycoproteins. The ECM of *V. carteri* is divided into the flagellar zone (FZ), boundary zone (BZ), cellular zone (CZ) and deep zone (DZ). The cellular zone has subzones CZ1, CZ2, CZ3 and CZ4. The deep zone has subzones DZ1 and DZ2. s, somatic cell; gonidium, reproductive cell. Dark grey: intracellular space of somatic and reproductive cells. The localization of the given ECM glycoproteins (blue) is indicated even if it is speculative or has been determined indirectly by analyzing certain ECM extracts. Further details can be found in the corresponding publications: ISG (Hallmann and Kirk, 2000), SSG185 (Ertl *et al.*, 1989), phI (Sumper *et al.*, 1993), phII (Sumper *et al.*, 1993), phS (Godl *et al.*, 1997), DZ-HRGP (Ender *et al.*, 1999), phDZ1 (Ender *et al.*, 2002) and phDZ2 (Ender *et al.*, 2002).

pherophorin-DZ2 (Ender *et al.*, 2002) and pherophorin-S (Godl *et al.*, 1997), followed. Recent protein sequence alignments demonstrated that SSG185 also belongs to the pherophorins. Thus, a whole protein family of seven pherophorins had been identified shortly after the turn of the millennium. The members of the pherophorin family typically have a dumbbell-like domain structure, with two globular domains separated by a rod-shaped hydroxyproline-rich domain (Godl *et al.*, 1995; Godl *et al.*, 1997; Sumper and Hallmann, 1998; Hallmann, 2003). In 2006, differential screenings of cDNA libraries identified another 15 pherophorins (Hallmann, 2006), and 4 years later, after the sequencing of the *V. carteri* genome, it was believed that there could even be 49 pherophorin-related genes in *V. carteri* (Prochnik *et al.*, 2010). Protein-sequence comparisons revealed that there are also 27 pherophorins in *Chlamydomonas reinhardtii*, the unicellular relative of *V. carteri* (Merchant *et al.*, 2007; Prochnik *et al.*, 2010).

Among the numerous pherophorins, fewer than 10 have been characterized in more detail (Sumper and Hallmann, 1998; Hallmann, 2003; Hallmann, 2006). All pherophorins investigated have been glycoproteins, i.e. they contained covalently attached oligosaccharide chains (glycans). The building blocks of these glycans are predominantly the

sugars arabinose and galactose, which indicates the O-linked glycosylation of serine, threonine and hydroxyproline. Notably, the amino acid hydroxyproline, produced by the post-translational hydroxylation of proline, is the dominant amino acid of the rod-shaped hydroxyproline-rich domain of pherophorins (Hallmann, 2003; Hallmann, 2006). Thus, in particular, this rod-shaped domain provides a substrate for extensive O-glycosylation. The O-linked sugars of pherophorins are also strongly sulfated, which made it possible to identify pherophorins by [<sup>35</sup>S]sulfate *in vivo* pulse-labeling studies (Wenzl and Sumper, 1981; Wenzl and Sumper, 1982). It was also demonstrated that some of the pherophorins contain a quite uncommon phosphodiester between two arabinose residues (Holst *et al.*, 1989; Godl *et al.*, 1997; Ender *et al.*, 2002). It has been speculated that the phosphodiester bridges are responsible for intermolecular cross links between the polysaccharide parts of pherophorins (Ender *et al.*, 2002). For two purified pherophorins, pherophorin-DZ1 and pherophorin-DZ2, polymerization has even been shown *in vitro*, producing an insoluble fibrous network (Ender *et al.*, 2002). The chemistry behind the polymerization remained unclear, however.

Only one of the characterized pherophorins, pherophorin-S, showed a quite unexpected characteristic for an ECM protein: it seemed to stay soluble without cross-linking with itself or other ECM components (Godl *et al.*, 1997). The 'S' of pherophorin-S thus stands for 'soluble'. What could be the role of a soluble ECM glycoprotein? Actually, all extracellular proteins must be bound to the ECM somehow in order to prevent diffusion into the surrounding pond water. The biochemical analysis of ECM fractions suggested a pherophorin-S localization in the deep zone (DZ), the innermost part of the *Volvox* spheroid (Figure 1), where it could be trapped by the surrounding ECM components (Godl *et al.*, 1997). Notably, pherophorin-S also contains phosphodiester bridges between arabinose residues (Godl *et al.*, 1997), even if the protein is soluble and does not show any cross-linking.

In this work, first we carried out a sequence database analysis to provide a current inventory of the existing pherophorin-related genes in *V. carteri*. The large family of pherophorin-related genes identified stresses the requirement of numerous different ECM glycoproteins to build, maintain and modify a complex ECM during the course of ontogenesis.

Following the pherophorin inventory, we focused on a particular pherophorin with a very special characteristic when it concerns an ECM protein: the soluble pherophorin-S. We show that expression of the pherophorin-S gene is enhanced by the sex-inducer protein, and we trace the synthesis, migration and concentration of fluorescence-tagged pherophorin-S *in vivo*. Moreover, we demonstrate that not only the sex-inducer protein but also

heat, salt and oxidative stress are able to increase pherophorin-S expression, and thus its local accumulation.

Finally, we provide a scenario that shows the action of the soluble ECM glycoprotein pherophorin-S together with lytic ECM enzymes to soften and then to dissolve the ECM. Pherophorin-S seems to be an ECM plasticizer involved in the hatching process and in the course of the intracorporeal fertilization of eggs inside sexual females.

## RESULTS

### Database analysis and inventory of pherophorin-related genes in *V. carteri*

After sequencing the *V. carteri* genome, it was believed that there are 49 pherophorin-related genes in *V. carteri* (Prochnik *et al.*, 2010). A recent search for genes that are computationally annotated as pherophorins in the *V. carteri* genome (v2.1) of Phytozome 12 (Goodstein *et al.*, 2012), however, resulted in 97 pherophorin genes. Our detailed BLAST searches (Altschul *et al.*, 1990; Johnson *et al.*, 2008; Boratyn *et al.*, 2013) of the *V. carteri* genome (v2.1) in Phytozome 12 using pherophorins as query sequences then revealed a total of 117 pherophorin genes. We thus found 20 pherophorin-related genes that are not annotated. Of the 117 pherophorin genes in the *V. carteri* genome, 68 genes are without a gene name and have not yet been described in a publication. Using an earlier nomenclature for pherophorins (Prochnik *et al.*, 2010), we therefore continue the gene designation and call these pherophorin-related genes *phV43–phV110*. An overview of all pherophorin-related genes of *V. carteri* is given in Table S1.

### Gene and mRNA sequences of pherophorin-S

In 1997, peptides, mRNA fragments and genomic fragments of pherophorin-S from *V. carteri* were investigated for the first time to obtain the complete amino acid sequence (Godl *et al.*, 1997). The coding sequence and the deduced amino acid sequence of pherophorin-S, but not the genomic sequence, have previously been deposited in the GenBank data library (accession no. Y07752). The gene of pherophorin-S (*phS*) has not been annotated in the current version 2.1 of the *V. carteri* genome, for unknown reasons. Nevertheless, we identified the *phS* gene on scaffold 4: the start codon is at nucleotide position 943321–943323 on the forward strand. Using the RNA-seq data available (Klein *et al.*, 2017) we identified a very short 5' untranslated region (5'-UTR) of only 10 bp, whereas there is a quite long 3'-UTR of 1803 bp (Figure S1). The genomic size is approximately 7 kb, including the UTRs and the promoter region. We also closed a previous sequence gap in exon 3 (Figure S1). The total pre-mRNA of *phS* is 6649 bp in length and contains seven introns. Once spliced, the mRNA is 3613 bp in length, but only

1800 bp of it represents a coding sequence. The fact that the 3'-UTR of *phS* covers half of the mRNA could indicate that the 3'-UTR contains regulatory regions that post-transcriptionally influence gene expression. The completed gene structure of *phS* is shown in Figure S2.

### Generation of *V. carteri* transformants with stable genomic integration of a chimeric *phS:yfp* gene

To visualize and track the expression and target location of pherophorin-S protein *in vivo*, a chimeric gene was constructed that allows for the expression of a fusion protein in which the C terminus of pherophorin-S is fused via a pentaglycine interpeptide bridge (Gly5) to a yellow fluorescent protein (YFP, mVenus) (Figure 2a). The chimeric *phS:yfp* gene is driven by the endogenous *V. carteri phS* promoter region and terminated by the endogenous *V. carteri phS* terminator region (Figure 2a) to allow for unaltered regulation of *phS* expression. The *yfp* coding sequence used has previously been codon-adapted for *C. reinhardtii* (Lauersen *et al.*, 2015) but also works well in *V. carteri* (Tian *et al.*, 2018). The *nitA*<sup>+</sup> transformants obtained were investigated for stable genomic integration of the co-transformed, chimeric *phS* gene by PCR amplification using their genomic DNA as a template (Figure 2b). The 309-bp fragments obtained indicate the presence of the chimeric *phS:yfp* gene in the corresponding transformants. The correct identity of the amplified DNA fragments was further confirmed by sequencing (Figure 2c).

### The sex-inducer protein increases the *phS* transcript abundance

The glycoprotein pherophorin-S has been identified as a radioactive band of approximately 100 kDa (on an 8% SDS polyacrylamide gel) in a pulse-chase experiment with [<sup>35</sup>S]-sulfate after treating vegetatively grown *Volvox* spheroids with the sex-inducer protein for 40 min (Godl *et al.*, 1997). It remained unclear, however, whether the sex-inducer enhances: (i) the transcription of the *phS* gene, with subsequent translation, protein glycosylation and sulfation; (ii) the translation of stored *phS* mRNA, with subsequent protein glycosylation and sulfation; (iii) the post-translational glycosylation of existing pherophorin-S protein, with subsequent sulfation; or (iv) the sulfation of hydroxyl groups in the sugar moiety of pre-existing glycosylated pherophorin-S.

To clarify this matter, we first analyzed whether the addition of the sex inducer triggers changes in the *phS* transcript abundance using a *Volvox* strain with an unmodified *phS* gene in its natural genomic environment (recipient strain TNit-1013). The quantitative real-time reverse transcriptase (RT)-PCR results in Figure 3(a) show that *phS* transcript abundance quickly increases about 12-fold in less than 1 h, and then the *phS* transcript abundance decreases very slowly; 14 h after sex induction it is still

about 7.5-fold higher than under the uninduced condition. The kinetics of the *phS* transcript abundance after sex induction match well with the kinetics of the [<sup>35</sup>S]sulfate-labelled pherophorin-S band in pulse-chase experiments after sex induction, indicating that the sex-inducer protein effectively enhances the transcription of *phS*, followed immediately by translation, protein glycosylation and sulfation.

The chimeric *phS:yfp* gene in our corresponding *Volvox* transformants also comprises the endogenous *phS* promoter. Thus, we checked by real-time RT-PCR whether the sex inducer also triggers changes in abundance of the chimeric *phS:yfp* transcript of transformants. In this experiment, transcript abundance was investigated 14 h after sexual induction and was compared with transcript abundance in cultures grown vegetatively. In fact, in all transformants the *phS:yfp* gene is sex inducible (Figure 3b). Compared with the uninduced condition, the induction factor varies between 3.5 and 7.5, however. Yet the *phS:yfp* transcript abundance in the transformant strain PhS-YFP-6-1 showed exactly the same induction behavior as the unmodified *phS* gene of the recipient strain TNit-1013 (Figure 3b). The results demonstrate that the required regulatory sequences for induction have not been destroyed or

cut off inadvertently during construction or genomic integration of the chimeric *phS:yfp* gene.

### Transformants produce fluorescence-tagged pherophorin-S protein

Stable transformants expressing the *phS:yfp* gene were examined with an LSM780 confocal laser scanning microscope (CLSM) for the presence of fluorescence. Our aim was to distinguish YFP fluorescence unequivocally from any autofluorescence. A major pigment contributing to autofluorescence is the chlorophyll in the chloroplast, which occupies a large portion of the cell's volume. Carotenoid pigments of the eyespot apparatus also show weak autofluorescence, however. Therefore, lambda scans were performed that allow for the separation of spatially overlapping emission signals. More precisely, fluorescence spectra of selected cellular and extracellular regions of sexually induced transformants were measured and compared, both with each other and with the known YFP spectrum (Kremers *et al.*, 2006). The same cellular and extracellular regions were also scanned in the untransformed, sexually induced recipient strain as a control. After excitation at 488 nm, only the fluorescence emitted from regions in the ECM of transformants (see below) peaked at

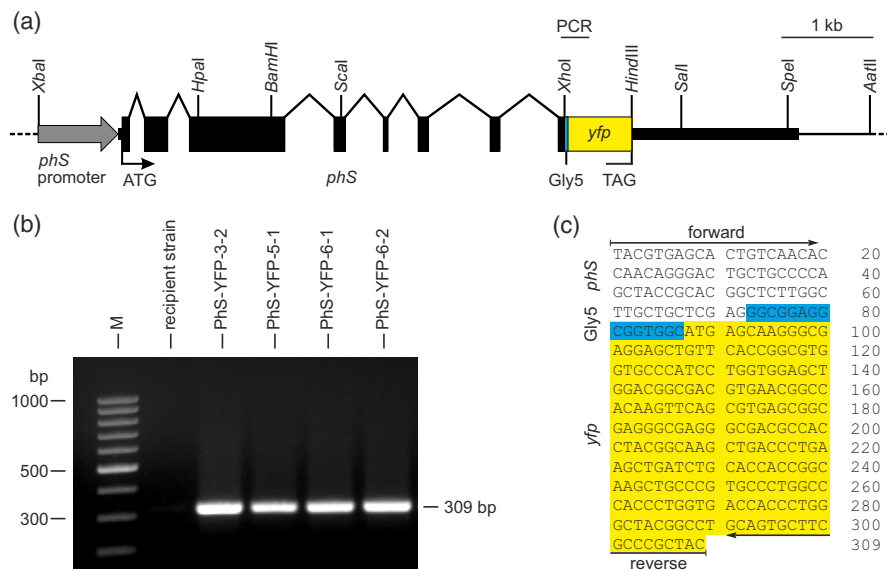


**Figure 2.** Schematic diagram of the transformation vector used and proof of integration of the chimeric gene construct into the recipient genome. (a) Vector pPhS-YFP carries a fragment of *Volvox carteri* genomic DNA containing the pherophorin-S gene (*phS*), including its seven introns, a short linker sequence, which codes for five glycines (Gly5), and the coding sequence of *yfp* (mVenus). The 5'- and 3'-flanking sequences, including the promoter region (grey arrow), the short 5' untranslated region (5'-UTR) and the long 3'-UTR, also come from the *phS* gene of *V. carteri*. The *yfp* (mVenus) coding sequence has been codon-adapted for *Chlamydomonas reinhardtii* (Lauersen *et al.*, 2015), but also works well in *V. carteri* (Tian *et al.*, 2018). (b) The stable integration of the transformed pPhS-YFP vector into the genome of transformants was verified by PCR amplification using genomic DNA of putative transformants as a template. The amplified fragment, which is indicated in (a) (PCR), is specific for the pPhS-YFP vector. Amplification of a fragment of an unaltered *phS* gene is excluded because one primer is located on the *yfp* coding sequence. The agarose gel electrophoresis shows the result with the untransformed recipient strain and four transformants obtained. The expected size of the amplified fragment was 309 bp. Lane M refers to the molecular weight marker. (c) Obtained sequence of the amplified fragments. The 309-bp PCR fragment contains 72 bp of exon 8 of *phS* (white background), a 15-bp fragment coding for a flexible pentaglycine interpeptide bridge (Gly5, blue background) and 222 bp of the *yfp* coding sequence (yellow background). The PCR primers used are indicated.

approximately 530 nm (Figure 4a). Both the position of the peak and the shape of the spectrum are typical for the YFP variant used (Kremers *et al.*, 2006).

### PhS:YFP protein synthesis increases up to 14-fold after sex induction

The *phS:yfp* transformants, which express the chimeric *phS:yfp* gene under control of the endogenous *phS* promoter, were analyzed under vegetative (uninduced) and sex-induced conditions for YFP fluorescence by CLSM, and the YFP fluorescence detected was quantified. To this end, fluorescent regions of the ECM (see below) were excited at 514 nm and the fluorescence signal was detected between 520 and 550 nm and quantified using ZEN BLACK (Figure 4b). Even vegetatively grown (uninduced) transformants revealed significant levels of YFP fluorescence. The PhS:YFP protein synthesis strongly increased after sex induction, however, and the induction factors ranged between 4 and 14 (Figure 4b). Fluorescence spectra (lambda scans) were conducted to ensure that the measured fluorescence originated only from YFP (Figure 4a). The increase of PhS:YFP protein synthesis after sexual induction of *phS:yfp* transformants roughly corresponds to the sex-induced increase of *phS* transcript abundance in these strains.

### In vivo localization of PhS:YFP protein during embryogenesis of sexual development

The pherophorin-S protein was previously identified in an ECM fraction of sexually induced *Volvox* spheroids (Godl

*et al.*, 1997). The ECM fraction has been assigned to the DZ (Figure 1); however, the identification of pherophorin-S in such an extract can only provide a very rough spatial resolution of its distribution in the organism. Moreover, earlier experiments dealt only with a single stage in development (Godl *et al.*, 1997). Therefore, it was our aim to characterize precisely both the spatial and temporal distributions of PhS:YFP in the corresponding transformants by CLSM. We focused on sexually induced algae because protein synthesis is strongly induced under these conditions, suggesting a role of pherophorin-S in sexual development. Moreover, the induction of *phS:yfp* transcript abundance by the addition of the sex inducer gives us a starting point for immediately following the strong increase in PhS:YFP protein synthesis, which can then be traced by CLSM. In order to distinguish unequivocally YFP fluorescence from autofluorescence in the CLSM, we verified the YFP fluorescence spectrum in the ECM of transformants (Figure 4a) and also investigated the untransformed *V. carteri* parent strain TNit-1013 for autofluorescence, as a control. As expected, strain TNit-1013 showed only weak chlorophyll autofluorescence in the chloroplast and very weak carotenoid autofluorescence in the eyespot, but no fluorescence in the ECM of any stage of vegetative or sexual development (Figure S3).

We added the sex-inducer protein to vegetatively grown *phS:yfp* transformants at the developmental stage shortly before the hatching of their juveniles to then follow the PhS:YFP synthesis and its distribution in the developing

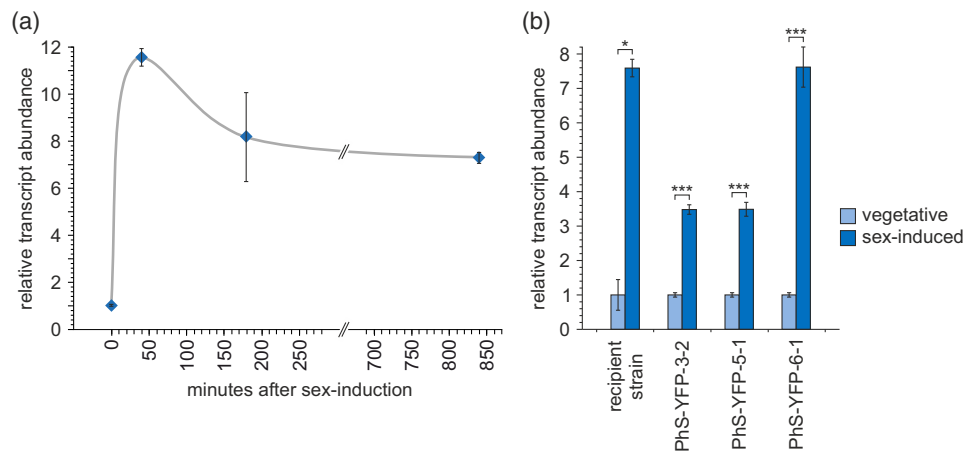


**Figure 3.** Inducibility of the *phS* promoter by the addition of the sex-inducer protein. (a) The induction kinetics of *phS* transcript abundance after the addition of the sex-inducer protein was investigated in a *Volvox* strain with an unmodified *phS* gene (including its endogenous promoter) in its natural genomic environment (recipient strain TNit-1013). Induction was started at 0 min by the addition of the sex-inducer protein. The data represent three biological replicates ( $n = 3$ ). Error bars indicate one standard deviation from the mean. (b) The sex inducibility of the *phS* transcript abundance of strain TNit-1013 was compared with the sex inducibility of the *phS:yfp* transcript abundance of three independent transformant strains, which integrated the chimeric *phS:yfp* construct into their genomes. The *phS:yfp* gene is driven by the endogenous *phS* promoter. To determine induction factors, transcript abundance was investigated 14 h after sexual induction (sex-induced) and set in relation to the transcript abundance in uninduced algae (vegetative). The sex-inducer protein was added at a concentration of  $10^{-12}$  M. Transcript abundance was analyzed by quantitative real-time RT-PCR. Oligonucleotide primer pairs were specific either for the unmodified *phS* gene (recipient strain TNit-1013) or for the chimeric *phS:yfp* gene (transformant strains). The relative transcript abundance was calculated using the  $2^{-\Delta\Delta C_t}$  method (Bustin, 2000; Pfaffl, 2001). The data represent three biological replicates with three technical replicates each. Error bars indicate one standard deviation from the mean. Asterisks indicate the level of statistical significance (Student's *t*-test, \* $P < 0.05$ , \*\* $P < 0.01$ , \*\*\* $P < 0.005$ ).

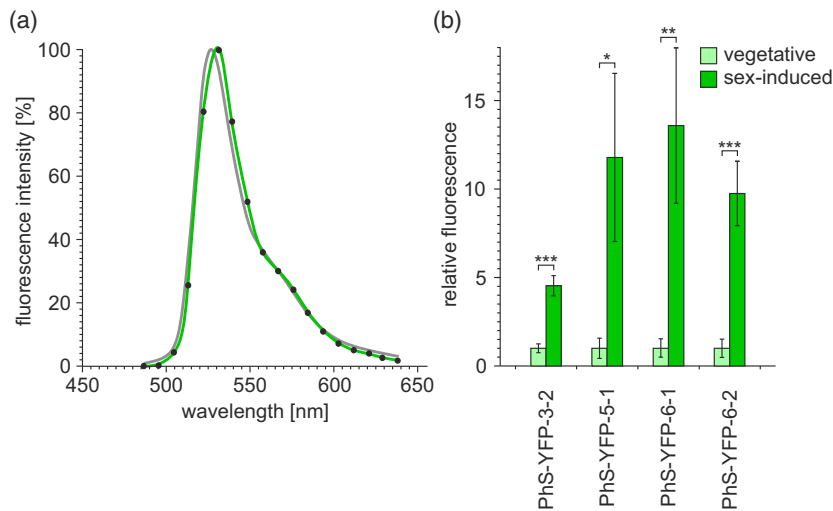


**Figure 4.** Verification of the YFP fluorescence spectrum in transformants and induction of PhS:YFP protein expression by the addition of the sex-inducer protein. (a) *In vivo* fluorescence spectrum (lambda scan) of an exemplary scanning region in the extracellular matrix (ECM) of *phS:yfp*-expressing transformants after sexual induction (green line). The fluorescence intensity was determined simultaneously in 18 different channels (with 9-nm steps) using a gallium arsenide phosphide (GaAsP) detector during excitation at 488 nm. The fluorescence intensity was plotted against the emission wavelength for each channel. Such lambda scans were carried out in all regions used for YFP fluorescence quantification and always resulted in the same intensity distribution. For comparison, a gray line shows a previously published YFP fluorescence spectrum (Kremers *et al.*, 2006). (b) Protein expression was quantified by measuring the *in vivo* fluorescence of PhS:YFP in the corresponding transformants. To determine induction factors, the YFP fluorescence was investigated 14 h after sexual induction (sex-induced) and set in relation to the YFP fluorescence of uninduced transformants (vegetative). To this end, ECM regions of interest were excited at 514 nm and the fluorescence signal was detected between 520 and 550 nm. Quantification was carried out using ZEN BLACK 2.1. The data represent three biological replicates with three or four technical replicates each. Error bars indicate one standard deviation from the mean. Asterisks indicate the level of statistical significance (Student's *t*-test, \* $P < 0.05$ , \*\* $P < 0.01$ , \*\*\* $P < 0.005$ ).

juveniles (Figure 5). Freshly hatched *Volvox* juveniles already produce fluorescent PhS:YFP protein (Figure 5a). The synthesized PhS:YFP protein appears at the surface of the spheroid in the ECM structures CZ1, CZ2 and CZ3, around the somatic cells, and begins to spread, probably by diffusion, into deeper ECM zones, i.e. into CZ4 (Figure 1). PhS probably cannot pass through the boundary zone (BZ), which seems to prevent PhS from diffusing into the surrounding medium (Figure 5a). Remarkably, the ECM structures CZ1, CZ2 and CZ3 around the immature gonidia (Figure 1) show hardly any fluorescence (Figure 5a). This indicates that the PhS:YFP protein is produced by somatic cells. Later in development, when the gonidia have matured inside the young adults and the first cleavage of embryogenesis lies ahead, the highest concentration of PhS:YFP is still detectable in the ECM structures CZ1, CZ2 and CZ3 of somatic cells, but the spread of PhS:YFP into deeper ECM zones increases continuously (Figure 5b). At this stage, small quantities of PhS:YFP protein also entered the ECM structures CZ2 and CZ3 around the mature gonidia, but not their CZ1. With advancing embryogenesis inside the adults, the PhS:YFP concentration in the cellular zones CZ2 and CZ3 around the dividing embryo increases, and in the 16-cell stage these zones show the strongest PhS:YFP fluorescence overall (Figure 5c). There is still no PhS:YFP fluorescence in the CZ1 around the embryo, however. This indicates that neither PhS:YFP nor pherophorin-

S are able to penetrate the CZ1 around embryos, i.e. the glycoprotein vesicle. In this context, it should be noted that dyes (e.g. 4',6-diamidino-2-phenylindole, DAPI) added to *Volvox* cultures from outside get into the interior of the spheroid, and also into the interior of the somatic cells, but they are not able to penetrate the CZ1 around gonidia or embryos and, thus, do not get into the interior of gonidia or embryos. These observations could imply that the CZ1 structure around gonidia or embryos constitutes a considerable barrier between the gonidium or embryo and its surrounding parent. The fact that the cells of the dividing embryo detach somewhat from the surrounding CZ1 makes it easier to see that the extracellular space between the plasma membranes of the embryonic cells and their surrounding CZ1 does not contain any notable levels of PhS:YFP fluorescence, even though there is a considerable presence of PhS:YFP fluorescence on the outside of the CZ1 (Figure 5c4). To illustrate this, we quantified the PhS:YFP fluorescence in this extracellular space under standard conditions and also produced CLSM images with overamplified YFP fluorescence (Figure S4). Moreover, there is also no notable PhS:YFP fluorescence inside the gonidia or embryos (Figures 5c4 and S4). Furthermore, this is in accordance with the RNA-seq data available (Klein *et al.*, 2017) that reveal an approximately 15-fold overexpression of *phS* mRNA in somatic cells compared with gonidia. Taken together, this shows that gonidia and dividing

embryos produce no notable quantities of PhS:YFP and that the observed PhS:YFP protein comes from the parent's somatic cells. During embryogenesis, PhS:YFP fluorescence also spread into the innermost ECM zone, the DZ (Figure 5c2). In return, the PhS:YFP fluorescence intensity in the cellular zones CZ2 and CZ3 around the somatic cells decreased. This also indicates that the production of PhS:YFP protein by the parent's somatic cells has declined at this stage, which corresponds to the induction kinetics of the *phS* transcript abundance (Figure 3a). Further on in their development the embryos undergo inversion inside their parent, and at the same time more and more PhS:YFP protein enters the ECM zones around the embryos and a shift of PhS:YFP protein from the CZ2 and CZ3 zones to the CZ1 zone emerges. Then, when egg cells within the juveniles, which are still inside their parent, become visible, the PhS:YFP fluorescence intensity at CZ1 gradually increases and CZ1 becomes the place with the highest concentration of PhS:YFP (Figure 5d). In return, the PhS:YFP fluorescence intensity in all other ECM zones gradually decreases, which indicates that PhS:YFP binds with high affinity to an unknown target at CZ1. The PhS:YFP protein eventually seems to stick firmly to the CZ1. There is (still) no detectable PhS:YFP fluorescence in the space between the egg-bearing juveniles and their surrounding CZ1 (Figure 5d4), and also not inside the egg-bearing juveniles. All the other ECM zones now contain only very low levels of PhS:YFP.

#### ***In vivo* localization of PhS:YFP protein during the hatching of egg-bearing juveniles**

The hatching of egg-bearing juveniles from their parent is a highly selective enzymatic process. In this process, birth canals for the juveniles must be formed (Kirk, 1998). To this end, lytic enzymes are secreted by the juveniles to specifically degrade the parental ECM (Fukada *et al.*, 2006), and these enzymes start with the disintegration of the CZ1 (Nishimura *et al.*, 2017). In addition, lytic enzymes are also secreted by the parental somatic cells. These enzymes accumulate in the parental ECM around the somatic cells and start to disintegrate it (Nishimura *et al.*, 2017). The birth canals are cooperatively formed by lytic enzymes secreted by the juveniles and those secreted by parental somatic cells (Nishimura *et al.*, 2017).

When the CZ1 is disintegrated by the lytic enzymes of the juveniles, the PhS:YFP protein seems to lose its footing in the ECM and once the juveniles hatch through the birth canals, a haze and streaks of fluorescent PhS:YFP protein leak from the holes. A significant level of PhS:YFP protein also sticks to the edges of the holes created (Figure 6), indicating that PhS:YFP protein might inhibit the autocatalytic repair mechanisms of the ECM (Ender *et al.*, 2002). At the edges of the created holes, PhS:YFP protein seems to mainly stick to the BZ and to the bottom of the somatic

cell sheet, which corresponds to CZ3. Thus, two fluorescent rings become visible at each birth canal, one at the outer rim and one at the inner rim of the holes in the somatic cell sheet (Figure 6).

#### ***In vivo* localization of PhS:YFP protein in matured egg-bearing adults**

After hatching, the (female) juveniles develop into adults with matured eggs and the somatic cells of the adults start to produce PhS:YFP protein, which then spreads into deeper ECM zones. The PhS:YFP protein accumulates continuously and becomes more or less evenly distributed across all ECM zones (Figure 7). There might be slightly more PhS:YFP protein in CZ3 than in the other ECM zones. On the whole, all eggs are surrounded by PhS:YFP-containing ECM. At this stage, the egg-bearing adult females are ready for fertilization by sperm. Contrary to the earlier situation around egg-bearing juveniles, in which CZ1 became the place with a strong concentration of PhS:YFP, there is not significantly more PhS:YFP accumulation in the immediate vicinity of the eggs than in other ECM zones.

#### **Overall model of the synthesis, migration and concentration of pherophorin-S**

Based on our numerous CLSM images of the different developmental stages of transformants expressing the *phS:yfp* gene, we developed an overall model of the synthesis, migration and concentration of pherophorin-S (Figure 8). After sexual induction, pherophorin-S is synthesized and excreted by somatic cells (Figure 8a). It then spreads into deeper ECM zones and enters the ECM structures CZ2 and CZ3 around the mature gonidia (Figure 8b). During embryogenesis, pherophorin-S concentration in the ECM zones CZ2 and CZ3 around the dividing embryo increases and pherophorin-S also spreads into the innermost ECM zones of the spheroid (Figure 8c,d). Then a shift of pherophorin-S protein from the CZ2 and CZ3 zones to the CZ1 around the embryos occurs, and CZ1 becomes the place with the highest concentration of pherophorin-S (Figure 8e). When the birth canals for the juveniles are formed, pherophorin-S spreads from CZ1 into the adjacent, pre-digested ECM around the parent's somatic cells (Figure 8f). Once the juveniles hatch through the birth canals created, a haze and streaks of pherophorin-S protein leak from the holes (Figure 8g). Pherophorin-S also sticks to the edges of the created holes (Figure 8g). After hatching, the (female) juveniles develop into adults with matured eggs and the adults' somatic cells start to produce pherophorin-S, which then spreads into deeper ECM zones (Figure 8h). Somewhat later, pherophorin-S is more or less evenly distributed across all ECM zones and all eggs are surrounded by pherophorin-S-containing ECM (Figure 8i). In the natural course, matured sperm packets released from sexual adult males

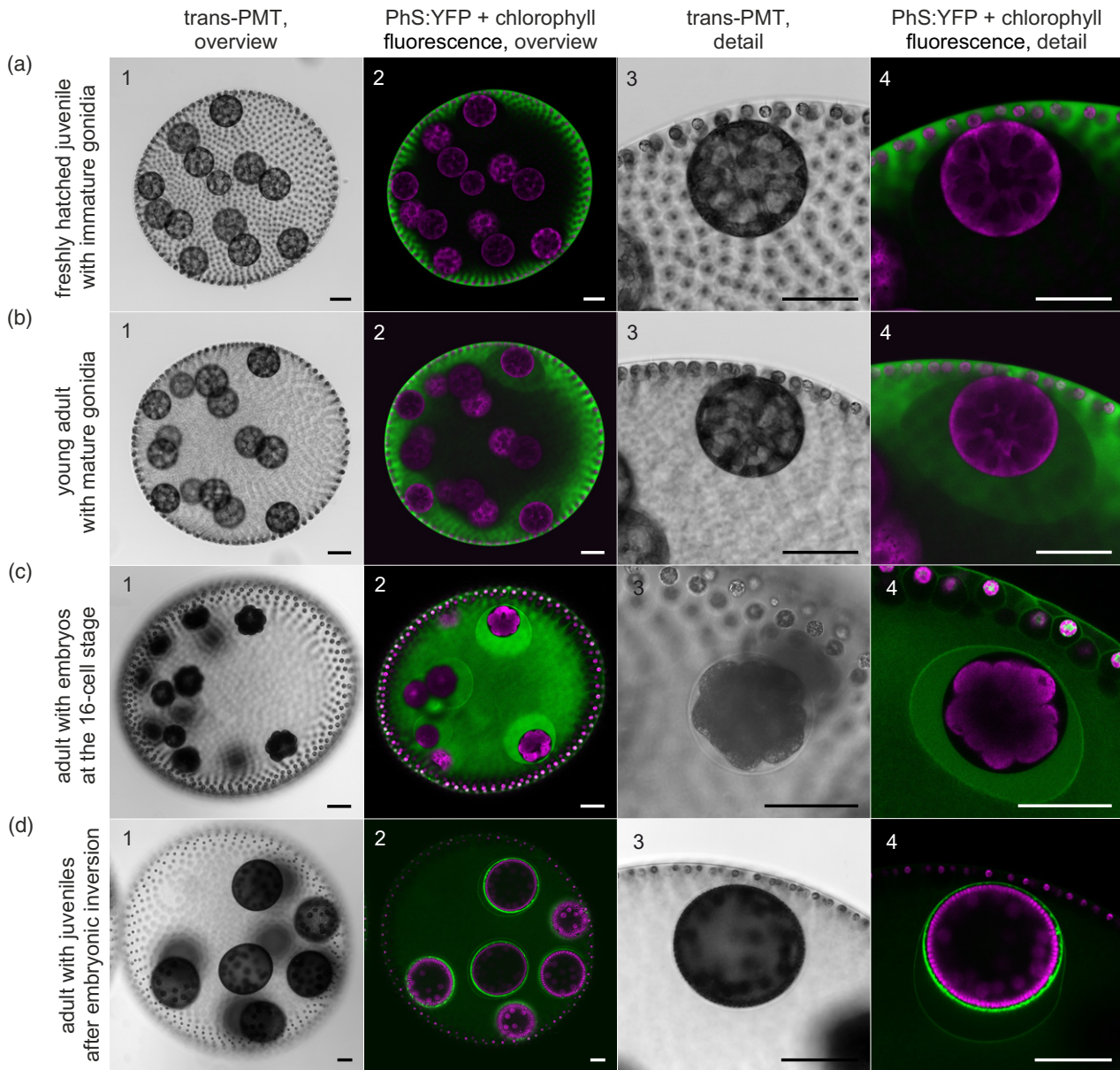


**Figure 5.** Localization of PhS:YFP in sexually induced *Volvox carteri* females before, during and after embryogenesis. The sex-inducer protein was added to transformants expressing the *phS:yfp* chimeric gene under the control of the wild-type *phS* promoter (strain PhS-YFP-6-1), and then they were analyzed *in vivo* for the localization of the PhS:YFP fusion protein. (a1–d1, column 1) Transmission-photomultiplier tube detection (trans-PMT): overview of whole organisms. (a3–d3, column 3) Trans-PMT: detailed view of one gonidium, embryo or juvenile, respectively, with its surrounding structures. (a2–d2, a4–d4, columns 2 and 4) Fluorescence images of the specimen shown in (a1–d1, a3–d3, columns 1 and 3). Overlay of YFP fluorescence of PhS:YFP protein (green) and chlorophyll fluorescence (magenta). (a1–a4) Freshly hatched juvenile with immature gonidia. (b1–b4) Young adult with mature gonidia. (c1–c4) Adult with embryos at the 16-cell stage. (d1–d4) Adult with (young) juveniles after embryonic inversion. The egg cells within the juveniles are already visible. Scale bars: 50  $\mu\text{m}$ .

will then dock onto the egg-bearing female adults, the sperm packets then break up into individual sperm and these sperm penetrate the ECM of the female to fertilize the eggs inside the female to produce diploid zygotes.

#### Stress-induced expression of PhS:YFP protein

In *Volvox*, the switch to the sexual mode of reproduction is not only triggered by the sex inducer but also by increased

temperatures, i.e. heat shock (Kirk and Kirk, 1986), which typically is a sign of a pond drying up in late summer. Only because the sexual cycle produces heavily walled, dormant zygotes (zygospores), the species can resist tough conditions like drought, heat and cold for a long period of time. In addition to increased temperatures, oxidative stress seems to trigger sexual development (Nedelcu and Michod, 2003; Nedelcu *et al.*, 2004). These findings suggest

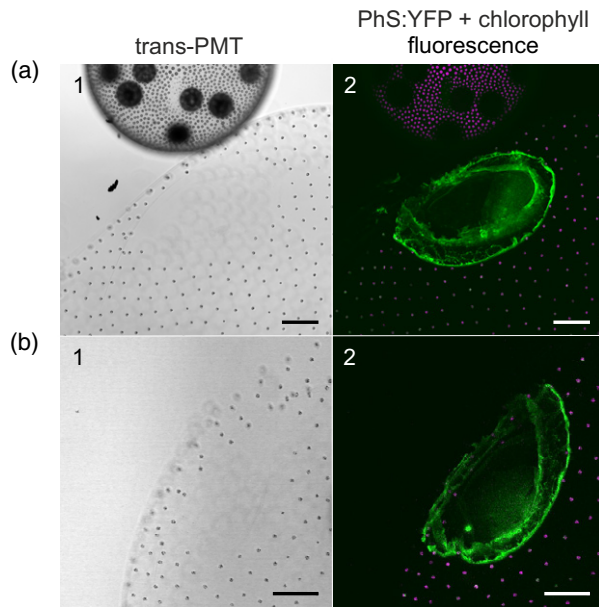


**Figure 6.** Localization of PhS:YFP in a sexually induced *Volvox carteri* female after the hatching of juveniles. The sex-inducer protein was added to transformants expressing the *phS:yfp* chimeric gene (strain PhS-YFP-6-1) and 48 h later, adult female algae were analyzed *in vivo* for the localization of the PhS:YFP fusion protein. (a1) Transmission-photomultiplier tube detection (trans-PMT): birth canal of an adult with a just-hatched juvenile above. The sexually induced juvenile contains egg cells. The hatched juvenile is approximately 520  $\mu\text{m}$  in diameter, whereas the birth canal has a diameter of only approximately 470  $\mu\text{m}$  (90% of the hatched juvenile). (b1) Trans-PMT: lateral view of a birth canal of an adult. (a2, b2) fluorescence images of the specimen shown in (a1, b1). Overlay of YFP fluorescence of PhS:YFP protein (green) and chlorophyll fluorescence (magenta). Scale bars: 100  $\mu\text{m}$ .

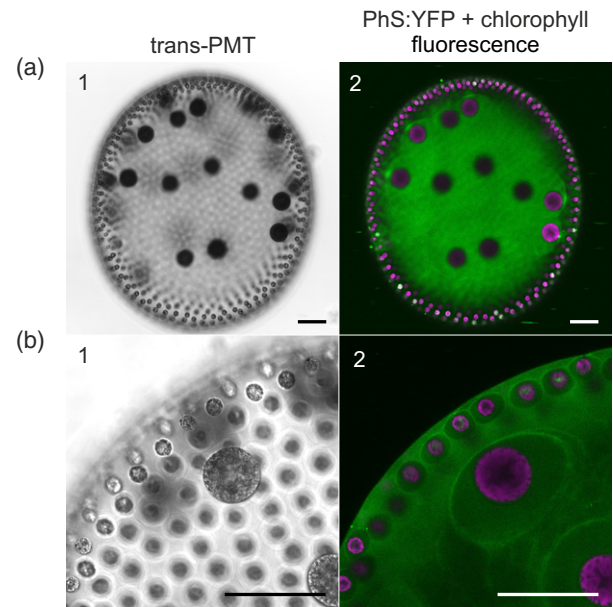


**Figure 7.** Localization of PhS:YFP in sexually developed *Volvox carteri* algae containing egg cells. The sex-inducer protein was added to transformants expressing the *phS:yfp* chimeric gene (strain PhS-YFP-6-1). After the hatching of sexually induced juveniles (with egg cells) and continued development, the adult sexually developed algae were analyzed *in vivo* for the localization of the PhS:YFP fusion protein (72 h after sexual induction). (a1) Transmission-photomultiplier tube detection (trans-PMT): sexually developed adult containing egg cells. (b1) Trans-PMT: detailed view of an egg cell with its surrounding structures. (a2, b2) fluorescence images of the specimen shown in (a1, b1). Overlay of YFP fluorescence of PhS:YFP protein (green) and chlorophyll fluorescence (magenta). Scale bars: 50  $\mu\text{m}$ .

a connection between a stress response and the induction of sexual development.

In view of the above, we examined whether the *phS* promoter is not only inducible by the sex inducer but also by stress stimuli. To this end, we exposed the transformants expressing the *phS:yfp* gene under the control of the wild-type *phS* promoter to heat-shock conditions, oxidative stress using  $\text{H}_2\text{O}_2$  and salt stress using NaCl. For comparison, the transformants were also induced by the sex inducer. Fourteen hours later, PhS:YFP expression was quantified by measuring the YFP fluorescence *in vivo*. All stress conditions had an enhancing effect on PhS:YFP expression (Figure 9). After treatment with 75 mM NaCl or 100  $\mu\text{M}$   $\text{H}_2\text{O}_2$  the PhS:YFP expression increased by a factor of 3–4. A further increase of the NaCl or  $\text{H}_2\text{O}_2$  concentrations did not result in an increased expression factor but had a negative impact on the shape and viability of the algae. In heat-shocked transformants, the expression of PhS:YFP was approximately 10 times higher than in untreated algae (Figure 9), which is similar to the situation after the addition of the sex-inducer protein, which resulted in a 14-fold induction.

## DISCUSSION

In the life of a *V. carteri* alga, ECM deposition begins after the completion of all cell divisions and after inversion, which is the process by which the embryo turns itself right-side-out at the end of embryogenesis. The ECM to be synthesized is dominated by a single HRGP family: the pherophorins (Godl *et al.*, 1995; Godl *et al.*, 1997; Sumper and Hallmann, 1998; Hallmann, 2003; Hallmann, 2006). When ECM deposition starts, the spheroid has a diameter of approximately 60  $\mu\text{m}$  (Kirk, 1998). Then, the juvenile alga not only needs to synthesize and secrete huge amounts of various HRGPs, which enable its massive organismal expansion, but the HRGPs also have to build the known region-specific, anatomically distinct ECM structures, and these structures must be able to expand together with the whole spheroid (Sumper and Hallmann, 1998; Hallmann, 2003; Hallmann, 2006). In an adult *V. carteri* alga at the stage shortly before the release of its matured juveniles, the ECM constitutes about 99% of the volume of the spheroid and its diameter is up to 2 mm, which corresponds to an increase in volume by a factor of more than 30 000 within roughly 24 h. This clearly

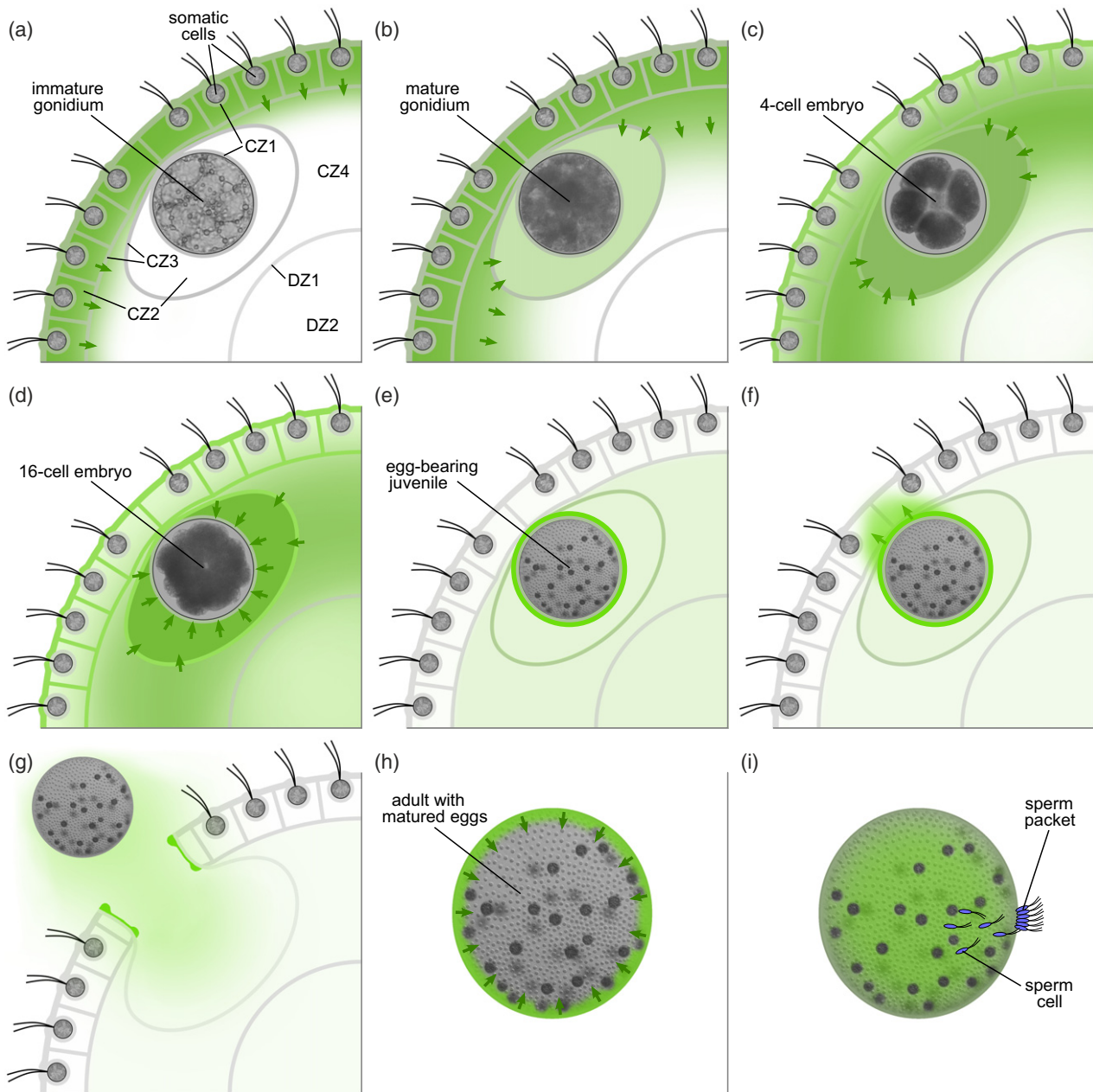


**Figure 8.** Model of the synthesis, migration and concentration of pherophorin-S during the development of sexual *Volvox carteri* females. Schematic cross section of a sexually developing *V. carteri* female, emphasizing the localization of pherophorin-S (green) in the given extracellular matrix (ECM) zones and the presumed flows of pherophorin-S (green arrows) during development. (a) Freshly hatched juvenile with immature gonidium. (b) Young adult with mature gonidium. (c) Adult with embryo at the four-cell stage. (d) Adult with embryo at the 16-cell stage. (e) Adult with juvenile after embryonic inversion; the juvenile contains egg cells. (f) Adult with egg-bearing juvenile; lytic enzymes start to digest birth canals into the parent's ECM. (g) Adult and its freshly hatched egg-bearing juvenile. (h) Adult with matured eggs. (i) Adult with matured eggs; a sperm packet released from a sexual adult male has docked onto the female and some sperm has begun to penetrate the ECM of the female. CZ, cellular zone; DZ, deep zone. The cellular zone has the subzones CZ1, CZ2, CZ3 and CZ4. The deep zone has the subzones DZ1 and DZ2.

demonstrates that the ECM must be a highly dynamic structure that allows for permanent expansion and remodeling. During the course of ontogenesis, ECM components also need to be locally removed to make room for new components. The most conspicuous ECM decomposition happens when large holes need to be formed to allow for

the hatching of the matured juveniles. But there is a big challenge: the ECM of the mother spheroid directly above the juvenile needs to be fully removed, whereas the ECM of the hatching juveniles must remain intact and completely unharmed. Therefore, it is not enough to simply produce large quantities of lytic enzymes to achieve this. A

similar situation exists when sperm need to penetrate the ECM of the egg-bearing female adults in order to reach the eggs inside the female for fertilization (Hallmann, 2011). The female's ECM needs to be softened to allow the sperm to swim to the eggs, but the sperm must not be harmed.

Not only do multicellular algae like *Volvox* face the need for digesting older ECM structures without impairing younger ECM structures, but even unicellular algae are confronted with such a situation. For example, soon after cell division, daughter cells of *C. reinhardtii* have to degrade their parental ECM (cell wall) to allow for hatching (Harris *et al.*, 2009). The corresponding lytic enzyme in *C. reinhardtii* is the vegetative lytic enzyme VLE (Matsuda *et al.*, 1995). As mentioned above, there are also 27 pherophorins in *C. reinhardtii* (Merchant *et al.*, 2007; Prochnik *et al.*, 2010). Among those, pherophorin PhC6 (Hallmann, 2006) exhibits the highest amino acid similarity with *Volvox* pherophorin-S (Figure S5). Remarkably, RNA-Seq data (Strenkert *et al.*, 2019) show that expression of the *phC6* mRNA peaks shortly before the hatching of the *C. reinhardtii* daughter cells (Figure S5). This could be a hint that the molecular repertoire for selectively removing older ECM structures (e.g. during hatching) evolved already in

unicellular ancestors of *V. carteri* and that already an ancestral lytic process required not only lytic enzymes but also ECM components related to pherophorin-S.

#### A scenario for the synergistic action of pherophorin-S and lytic ECM enzymes

Aside from the HRGP pherophorin-S, two lytic enzymes seem to be of importance for the ECM degradation of the hatching process in *V. carteri*: VheA (Fukada *et al.*, 2006) and Lsg2 (Nishimura *et al.*, 2017) (Figure 10). The protease VheA is secreted by the juveniles (Figure 10a) and is able to disintegrate the CZ1 around the juveniles (Fukada *et al.*, 2006; Nishimura *et al.*, 2017). It should be noted that this ECM zone is misleadingly also called 'gonidial vesicle', even though it contains no membrane and, moreover, is not only present at the gonidial stage but also at the subsequent stages, until its disintegration shortly before the hatching of the formed juveniles. As we show in this paper, the HRGP pherophorin-S accumulates at the CZ1 around the juveniles, the 'gonidial vesicle', and seems to adhere to this ECM zone (Figures 5d and 10a). The strong concentration of pherophorin-S at the CZ1 (Figure 5d) indicates a very high affinity of pherophorin-S for a component of the CZ1. The second lytic ECM enzyme, Lsg2, is secreted only by the parental somatic cells (Figure 10a) (Nishimura *et al.*, 2017). Once VheA disintegrates the CZ1 around the juveniles (Figure 10b), pherophorin-S becomes liberated (Figure 10c). It is then located in the liquefied space around the juveniles together with VheA and disintegrated ECM components (Figure 10c). While this is happening, Lsg2 diffuses into the ECM that surrounds the somatic cells and pre-digests this parental ECM.

Why seems the action of the two lytic enzymes to be not enough for making holes into the parental ECM under natural conditions? Earlier considerations about the generation of holes for hatching included only the lytic enzymes VheA (Fukada *et al.*, 2006) and Lsg2 (Nishimura *et al.*, 2017), but the corresponding assays for confirmation worked only under non-physiological conditions that included pre-heating of the substrate algae at 55°C, which kills the cells and denatures the proteins, and the addition of very high lytic enzyme concentrations that resulted in an atypical, destroyed-looking phenotype (Nishimura *et al.*, 2017). Under natural *in vivo* conditions, large numbers of new HRGPs are synthesized and secreted by somatic cells at any developmental stage after embryonic inversion (Sumper and Hallmann, 1998; Hallmann, 2003). Thus, the ECM production does not stop before hatching. In addition, autocatalytic cross-linking of at least two HRGPs, the pherophorins DZ1 and DZ2, allows for ECM self-assembly and even healing of ECM damage (Ender *et al.*, 2002), a process that counteracts the formation of birth canals for the hatching of the juveniles. A reasonable function of the soluble pherophorin-S could thus be that it hampers ECM

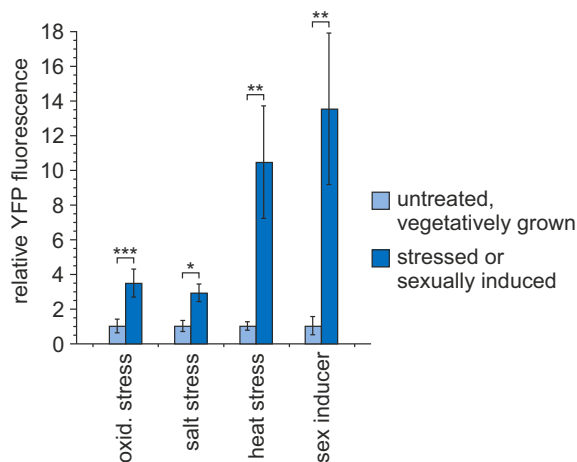


**Figure 9.** Induction of PhS:YFP protein expression after stress stimulation or the addition of the sex inducer. Transformants expressing the *phS:yfp* chimeric gene under the control of the wild-type *phS* promoter (strain PhS-YFP-6-1) were subject to stress stimulation (oxidative, salt and heat stress) or sexual induction with the sex-inducer protein. Then the expression of the PhS:YFP protein was analyzed *in vivo* by quantification of the YFP fluorescence and the results were compared with the YFP fluorescence obtained from untreated, vegetatively grown algae. Oxidative stress was generated by the addition of 100  $\mu\text{M}$   $\text{H}_2\text{O}_2$ , salt stress was produced by adding 75 mM NaCl and heat stress was caused by increasing the temperature to 42.5°C for 100 min and then to 45°C for 20 min. Sex induction was performed as described above. In the confocal laser scanning microscope (CLSM) analysis, regions of interest were excited at 514 nm and the fluorescence signal was detected between 520 nm and 550 nm. Quantification was carried out using ZEN BLACK 2.1. The data represent three biological replicates, with three or four technical replicates each. Error bars indicate one standard deviation from the mean. Asterisks indicate the level of statistical significance (Student's *t*-test, \* $P < 0.05$ , \*\* $P < 0.01$ , \*\*\* $P < 0.005$ ).

polymerization as an inhibitor. Parts of pherophorin-S could resemble the corresponding parts of cross-linked pherophorins, but pherophorin-S cannot then be integrated into the HRGP meshwork. In this way, pherophorin-S could act like an ECM plasticizer.

At the parental ECM position, right above the juvenile, the two lytic ECM enzymes and pherophorin-S coincidentally take effect on the ECM meshwork. The simultaneous presence of these three ECM components seems to create the weakest area in the parental ECM (Figure 10d). There, the ECM first softens then begins to dissolve, and, after a short time, holes develop (Figure 10e). These birth canals allow for the hatching of the juveniles (Figure 10f).

When sperm need to pass through the ECM of female adults to reach the eggs for fertilization, the female's ECM also needs to be softened to allow the sperm to penetrate the spheroid. This agrees well with our finding that pherophorin-S is distributed more or less evenly across all ECM zones of egg-bearing females (Figure 7). Thus, at this stage in development, pherophorin-S again seems to act as an ECM plasticizer. At this developmental stage, the simultaneous presence of lytic enzymes has not been investigated but can be expected.

#### Increased pherophorin-S levels after stress stimuli and sex induction might allow for faster ECM remodeling

As we showed, pherophorin-S protein levels increase by a factor of 3–4 after the application of oxidative stress or salt stress (Figure 9). Moreover, pherophorin-S expression was even found to be approximately 10 times higher in heat-stressed algae compared with untreated algae, which was similar to the induction factor after addition of the sex-inducer protein, which resulted in a 14-fold induction (Figure 9). Our heat-stress conditions were as described earlier (Kirk and Kirk, 1986), and these conditions mean that the treated algae switch from vegetative to sexual development. As expected, the heat-treated PhS:YFP-expressing transformants also produced egg-bearing sexual progeny at a rate of approximately 98%. The heat-induced switch to sexual development requires a remodeling of the ECM (Sumper and Hallmann, 1998), and for this to happen ECM components need to be modified or removed to make room for new ECM components. A similar ECM remodeling seems to be triggered by the addition of the sex-inducer protein (Sumper and Hallmann, 1998; Hallmann, 2003), and it is quite obvious that other external stimuli, like oxidative stress or salt stress, also effect changes of the ECM structures. External (stress) stimuli indicate environmental changes that can require immediate adaptation to reduce a disadvantage, to obtain a competitive advantage or even to protect the life of the alga. Two of the stresses that we tested, i.e. heat stress (Kirk and Kirk, 1986) and oxidative stress (Nedelcu and Michod, 2003; Nedelcu *et al.*, 2004), are also able to induce the switch to sexual

development, which is otherwise triggered by the sex inducer. Therefore, the induction of pherophorin-S synthesis by these stresses could also be a secondary effect caused by the induction of the sexual pathway, which also leads to ECM remodeling. The reaction speed of any ECM remodeling could be increased by increasing the synthesis rate of the components required for ECM reconstruction, which include ECM plasticizers (e.g. pherophorin-S), ECM-degrading enzymes (e.g. VheA and Lsg2) and structural building blocks of the ECM (i.e. different HRGPs).

Remarkably, highly dynamic ECM remodeling is not only found in *Volvox* or other multicellular (green) algae, but also in animals (Lu *et al.*, 2011; Matusiewicz, 2011; Sonbol, 2018). As in *Volvox*, animal ECMs are modified and remodeled throughout development, and most conditions of stress induce intense ECM remodeling (Jean *et al.*, 2011). When the ECM dynamics of animal tissues become deregulated or disturbed, it leads to various defects and diseases, including cancer (Lu *et al.*, 2011; Matusiewicz, 2011; Chakravarthy *et al.*, 2018; Sonbol, 2018). The further investigation and comparison of algae and animal ECM characteristics could help to shed more light on the fundamental biochemical requirements for dynamic ECM remodeling and its evolutionary development.

#### CONCLUSION

Our results provide insights into how an ECM zone that surrounds the developing progeny is remotely affected by the distantly located parental somatic cells. Based on the characteristics of the pherophorin-S glycoprotein, its synthesis by somatic cells, its conspicuous migration and its localized concentration in the ECM around prehatching juveniles, we conclude that pherophorin-S is likely to act as an ECM plasticizer. Pherophorin-S probably acts together with known lytic ECM enzymes to soften and then to dissolve the ECM to allow for the hatching of juveniles. Softening of the ECM by pherophorin-S could also help sperm in the course of the intracorporeal fertilization of eggs inside sexual females. The observed increase of pherophorin-S levels after sex induction and stress stimuli might allow for an accelerated ECM remodeling, which includes the quick removal of existing ECM components to make room for newly synthesized ECM components. The more dynamic the ECM remodeling is, the more adaptable the organism is when environmental conditions change.

#### EXPERIMENTAL PROCEDURES

##### Strains and culture conditions

The wild-type *Volvox carteri f. nagariensis* strain Eve10 (female), which originates from Japan, has been described previously (Starr, 1969; Starr, 1970; Kianianmomeni *et al.*, 2008). A non-revertible nitrate reductase-deficient (*nitA*<sup>-</sup>) descendant of Eve10,

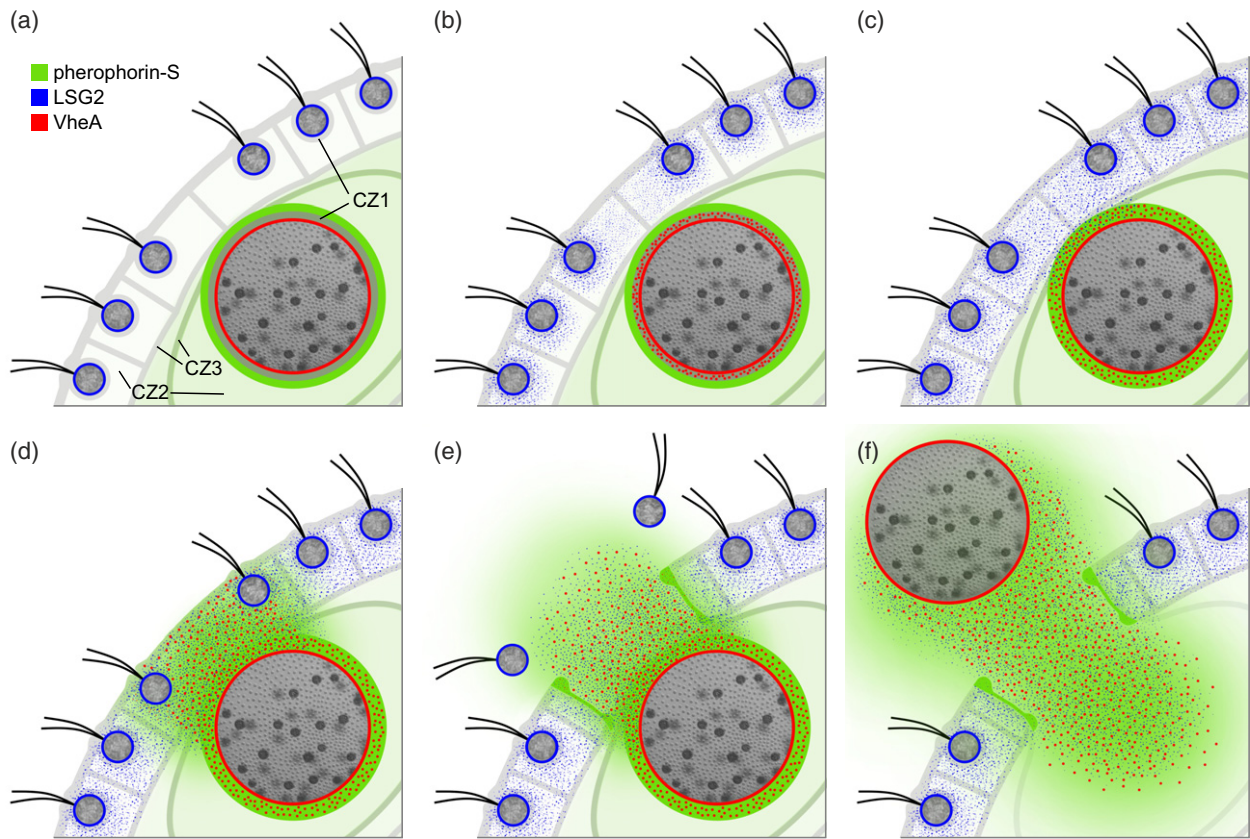


**Figure 10.** Model of the synergistic effects of pherophorin-S and lytic extracellular matrix (ECM) enzymes during the hatching of juveniles. Schematic cross section of an adult *Volvox carteri* female with an egg-bearing juvenile during the hatching process. The depiction emphasizes the localization of pherophorin-S (green) and the lytic enzymes LSG2 (blue) and VheA (red). (a) Pherophorin-S coats the CZ1 around the juvenile, LSG2 is secreted by the parental somatic cells and VheA is secreted by the juvenile. (b) Both LSG2 and VheA spread into the surrounding ECM zones. (c) VheA disintegrates the CZ1 around the juvenile and thereby releases pherophorin-S into the emerging liquid space around the juvenile. LSG2 spreads deeper into the surrounding ECM zones and pre-digests these zones. (d) Where the occurrence of pherophorin-S, LSG2 and VheA overlap, the ECM begins to soften and then to dissolve. Somatic cells of the somatic cell layer above the juveniles are liberated into the surroundings. (e) The progressing ECM dissolution creates birth canals for the juveniles. (f) The juveniles hatch through the created birth canals. The model includes earlier results regarding ECM structures (Kirk *et al.*, 1986; Hallmann, 2003) and lytic ECM enzymes (Fukada *et al.*, 2006; Nishimura *et al.*, 2017).

strain TNit-1013 (Tian *et al.*, 2018), was used as a recipient strain for transformation experiments. The recipient strain was grown in standard *Volvox* medium (Provasoli and Pintner, 1959), supplemented with 1 mM ammonium chloride ( $\text{NH}_4\text{Cl}$ ) as a nitrogen source. Transformants with a complemented nitrate reductase gene were grown in standard *Volvox* medium without ammonium chloride. Cultures were grown at 28°C in a cycle of 8 h dark/16 h cool fluorescent white light (Starr and Jaenicke, 1974) at an average of approximately  $100 \mu\text{mol photons m}^{-2} \text{s}^{-1}$  photosynthetically active radiation (PAR) in glass tubes or Fernbach flasks. The glass tubes had caps that allow for gas exchange. Fernbach flasks were aerated with approximately  $50 \text{ cm}^3$  sterile air per min.

### Vector construction

Standard cloning methods (Sambrook and Russell, 2001) and overlap extension PCR (Higuchi *et al.*, 1988) were used for the construction of the expression vector, plasmid pPhS-YFP (Figure 2), carrying the chimeric *phS:yfp* gene. Plasmid pPhS-YFP contains a 5.7-kb fragment of *V. carteri* genomic DNA harboring the *phS* gene under the control of its own promoter (Figure S6). The fragment begins 0.9 kb upstream of the *phS* start codon and ends

right in front of the *phS* stop codon. It is flanked by an artificial *Xba*I site and an artificial *Xho*I site (Figures 2 and S6). Our sequencing results of the genomic *phS* sequence (Figure S1) coincide with the corresponding *phS* sequence of the published *V. carteri* genome (v2.1, scaffold 4, nucleotides 942447–950704) (Prochnik *et al.*, 2010) in Phytozome 12.1.6 (Goodstein *et al.*, 2012); however, the *phS* gene in genome version 2.1 contained a 141-bp sequence gap, which we closed (Figure S1). For unknown reasons, in genome version 2.1 no gene model has been created for the *phS* gene on scaffold 4 (nucleotides 942447–950704).

In order to facilitate the fusion of the genomic *phS* fragment with *yfp* (mVenus), artificial *Xho*I and *Hind*III sites were added on both sides of the intronless *yfp* reporter gene (Kremers *et al.*, 2006; Lauersen *et al.*, 2015) and, simultaneously, a short linker sequence that codes for a flexible pentaglycine interpeptide bridge was inserted in front of the *yfp* gene (Figures 2 and S6). The 0.7-kb *yfp* sequence was previously codon-adapted to *C. reinhardtii* (Lauersen *et al.*, 2015). The chimeric *phS:yfp* gene is terminated by the natural *phS* terminator region harbored within a 2.6-kb fragment of *V. carteri* genomic DNA (Figures 2 and S6). The fragment is flanked by natural *Hind*III and *Aat*II sites and contains the

complete *phS* 3'-UTR (1.8 kb) and 0.8 kb of downstream sequence (Figures 2 and S6).

The chimeric *phS:yfp* gene was assembled within the pBlue-script II SK(-) (Stratagene, now Sigma-Aldrich, <https://www.sigmaaldrich.com>) vector backbone.

### Stable nuclear transformation of *V. carteri* by particle bombardment

Stable nuclear transformation of *V. carteri* strain TNit-1013 was performed as described previously (Schiedmeier *et al.*, 1994), but with some modifications and using a Biolistic PDS-1000/He (Bio-Rad, <https://www.bio-rad.com>) particle gun (Hallmann and Wodniok, 2006). The target algae were co-bombarded with the selectable plasmid pVcNR15 (Gruber *et al.*, 1996), carrying the *V. carteri* nitrate reductase gene, and the non-selectable plasmid pPhS-YFP. Plasmid pVcNR15 is able to complement the nitrate reductase deficiency of the recipient strain. For the selection of transformants, the nitrogen source of the *Volvox* medium was switched from ammonium to nitrate and the algae were then incubated under standard conditions in Petri dishes (9 cm in diameter) filled with a volume of approximately 35 ml of liquid medium. After incubation for at least 6 days, the Petri dishes were inspected for green and living transformants.

### Isolation of genomic DNA

Genomic DNA was isolated from *Volvox* algae as previously described (Edwards *et al.*, 1991), with minor modifications. The purity of DNA was determined by measuring the 260/280 and 260/230 ratios using a Nanodrop 1000 (ThermoFisher Scientific, <https://www.thermofisher.com>) UV-Vis spectrophotometer. For the 260/280 ratio a value of approximately 1.8 indicated pure DNA and for the 260/230 ratio it was a value of 2.0–2.2. The DNA was quantified by absorbance at 260 nm. The quality of DNA was further verified by agarose gel electrophoresis.

### Genomic PCR

In order to verify the stable integration of the chimeric *phS:yfp* gene into the genome of *V. carteri* transformants, PCR reactions with genomic DNA as a template were carried out as previously described (Lerche and Hallmann, 2009; Lerche and Hallmann, 2013; Lerche and Hallmann, 2014) using a gradient PCR thermal cycler (Mastercycler Gradient; Eppendorf, <https://www.eppendorf.com>). The PCR conditions were as follows: initial denaturation at 95°C for 2 min followed by 40 cycles of 95°C for 30 sec, 55°C for 30 sec and 72°C for 30 sec; the final elongation step was at 72°C for 5 min. The oligonucleotide primers used were 5'-TACGTGAGCACTGTCAACA-3' and 5'-GTAGCGGGCGAAGCACTGC-3' (Figure 2c). The size of PCR products was analyzed by agarose gel electrophoresis.

### Isolation of total RNA

Approximately 250 µl of concentrated frozen algae were disrupted in 2-ml tubes containing 10 1-mm silica beads (ThermoFisher Scientific) in 1 ml of phenol-based TRI Reagent (Sigma-Aldrich) using a tissue homogenizer (Precellys Evolution Homogenizer; Bertin Instruments, <https://www.bertin-instruments.com>). Cells were homogenized by running three cycles of 20 sec at 10 000 rpm with a 10-sec cool-down period between cycles. For the extraction of total RNA, 300 µl of trichloromethane was added to the homogenate. RNA precipitation and RNA purification was performed as previously described (Lerche and Hallmann, 2009; Lerche and Hallmann, 2013; Kianianmomeni *et al.*, 2014; Lerche and Hallmann,

2014). The purity of RNA was determined by measuring the 260/280 and 260/230 ratios using a Nanodrop 1000 UV-Vis spectrophotometer (ThermoFisher Scientific). For the 260/280 ratio a value of approximately 2.0 indicated pure RNA, and for the 260/230 ratio a value of approximately 2.0–2.2 was indicative. The RNA was quantified by absorbance at 260 nm. The quality of RNA was further verified by agarose gel electrophoresis.

### Quantitative real-time RT-PCR

Quantitative real-time RT-PCRs were carried out using the SensiFAST SYBR Hi-Rox One-Step Kit (Bioline, <https://www.bioline.com>) and the CFX96 Touch Real-Time PCR Detection System (Bio-Rad). Three biological replicates with three technical replicates each were performed for every experimental condition. The products of all quantitative real-time RT-PCR reactions were analyzed by agarose gel electrophoresis to ensure the amplification of a single, specific product of the correct size. For reverse transcription and amplification of a fragment of the chimeric *phS:yfp* transcript, the total RNA of transformants was used as a template and the oligonucleotide primers used were 5'-TCGACTTGTGCTGGGCTTC-3' and 5'-CGGTGAACACTCCTCGC-3'. The amplified fragment was expected to be 147 bp in length containing 31 bp of *phS* exon 7, 67 bp of *phS* exon 8, 6 bp of an artificial *HindIII* restriction site, a 15-bp fragment coding for a flexible pentaglycine interpeptide bridge (Gly5) and 28 bp of the *yfp* (*mVenus*) coding sequence, which was codon adapted for *C. reinhardtii* previously (Lauersen *et al.*, 2015). For reverse transcription and amplification of a fragment of the wild-type *phS* transcript, total RNA of the untransformed recipient strain was used as a template and the oligonucleotide primers used were 5'-TCGACTTGTGCTGGGCTTC-3' and 5'-ATCTTAAGCTTACAGCAAGCC-3'. The amplified fragment was expected to be 110 bp in length, containing 31 bp of *phS* exon 7 and 79 bp of *phS* exon 8. For reverse transcription and the amplification of a fragment of the reference transcript (*eef1*, eukaryotic translation elongation factor 1 $\alpha$ 2 gene), the total RNA of transformants or the untransformed recipient strain was used, respectively. The oligonucleotide primers used were 5'-GACGATTGCATGCCACTAAG-3' and 5'-ATCAGCAGGCACACATCAGC-3' and the amplified fragment was expected to be 132 bp in length. Previously, the *eef1* gene has been established as a suitable reference gene for quantitative real-time RT-PCRs in *V. carteri*, particularly when vegetative and sex-induced algae are compared with each other (Kianianmomeni and Hallmann, 2013). The cycling conditions in the CFX96 Touch™ Real-Time PCR Detection System were as follows: reverse transcription was at 50°C for 20 min, followed by polymerase activation at 95°C for 2 min and 40 cycles of DNA amplification with 95°C for 7 sec, 55°C for 12 sec and 72°C for 7 sec. Melting curves were recorded to check for the amplification of a single specific product. The relative transcript abundance was calculated using the 2<sup>- $\Delta\Delta$</sup>  method (Bustin, 2000; Pfaffl, 2001).

### Confocal laser scanning microscopy

For life cell imaging, algae were grown under standard conditions and examined using an inverted LSM780 confocal laser scanning microscope (Carl Zeiss GmbH) equipped with 63 $\times$  LCI Plan-Neofluar and 10 $\times$  Plan-Apochromat objectives (Carl Zeiss GmbH, <https://www.zeiss.com>). The confocal pinhole diameter of the microscope was set to 1 Airy unit, which corresponds to an optical section of 0.8 µm. The fluorescence of the YFP within the PhS:YFP fusion protein was excited by an argon-ion (Ar<sup>+</sup>) laser at 514 nm, we used an MBS 458/514 main beam splitter and the fluorescence was detected between 520 and 550 nm. The fluorescence of

chlorophyll was detected at 650–700 nm. Fluorescence intensity was recorded in bidirectional scan mode for YFP and chlorophyll in two channels simultaneously. Transmission images were obtained in a third channel using a transmission-photomultiplier tube detector (trans-PMT). Images were captured with a bit depth of 12 bits per pixel (4096 gray levels) and analyzed using ZEN BLACK 2.1 digital imaging software (ZEN 2011; Carl Zeiss GmbH). Image processing and analysis was performed with FIJI (IMAGEJ 1.51w) (Schindelin *et al.*, 2012). The lambda scan function of ZEN and a gallium arsenide phosphide (GaAsP) QUASAR photomultiplier detector (Carl Zeiss GmbH) were used to produce simultaneous 18-channel read-outs. Emission spectra between 486 and 637 nm were recorded for each pixel with a spectral resolution of 9 nm using a main beam splitter MBS 488 and 488-nm laser light for excitation. After data acquisition, spectral analysis for the regions of interest was performed, which even allows for the separation of heavily overlapping emission signals.

For the quantification of the sex-induced expression of the PhS:YFP fusion protein, vegetatively grown cultures of transformants with a density of 10 spheroids per ml, and at the stage shortly before the hatching of juveniles, were treated by the addition of the sex-inducer protein at a concentration of  $10^{-12}$  M. For quantification of the PhS:YFP expression after stress stimulation, transformants were instead treated with 100  $\mu$ M H<sub>2</sub>O<sub>2</sub> (oxidative stress), 75 mM NaCl (salt stress) or they were incubated at 42.5°C for 100 min followed by 45°C for 20 min (heat stress). After 14 h of further incubation under standard conditions, the algae were concentrated on a 100- $\mu$ m mesh nylon screen and analyzed by confocal laser scanning microscopy, as described above. All images were taken with the same set-up and with the same settings. To facilitate the comparability of the images, the focal plane was always adjusted to the center plane of the spherical algae, which was achieved by searching in z-direction for somatic cells at the furthest distance from the center of the spheroid. Regions of interest with 4000 pixels were manually selected, while taking care that the fluorescence signal was uniform and evenly distributed within the given area. Quantification of PhS:YFP protein expression was carried out using ZEN BLACK 2.1. Three biological replicates with three or four technical replicates each were performed for every experimental condition.

## ACKNOWLEDGEMENTS

We are grateful to Thorsten Seidel for support with the CLSM, Eva Laura von der Heyde for sharing her expertise on *yfp*-localization in *Volvox*, Olaf Kruse for providing the codon-adapted *yfp* and Kordula Puls for technical assistance. This work was supported by Bielefeld University.

## AUTHOR CONTRIBUTIONS

BH conducted the experimental and analytical work and wrote the first draft of the article. AH (corresponding author) conceived and coordinated the study, critically evaluated the data, and finalized the article. Both authors read and approved the final version for publication.

## CONFLICT OF INTEREST

The authors declare that they have no conflicts of interest.

## DATA AVAILABILITY STATEMENT

All data generated or analyzed during this study are included in this article and its supplementary information files. Plasmids are available upon request.

## SUPPORTING INFORMATION

Additional Supporting Information may be found in the online version of this article.

**Figure S1.** Genomic sequence of the *Volvox carteri* *phS* gene.

**Figure S2.** Schematic structure of the *phS* gene, *phS* mRNA and pherophorin-S protein.

**Figure S3.** Absence of autofluorescence from the ECM of the untransformed *Volvox carteri* parent strain TNit-1013.

**Figure S4.** Absence of PhS:YFP fluorescence from the extracellular space between the plasma membranes of the embryonic cells and their surrounding CZ1.

**Figure S5.** Pherophorin-S of *Volvox carteri* is similar to the hatching-specific pherophorin PhC6 expressed in *Chlamydomonas reinhardtii*.

**Figure S6.** Sequence of the chimeric *phS:yfp* gene in vector pPhS-YFP.

**Table S1.** Overview of pherophorin-related genes in *Volvox carteri*.

## REFERENCES

- Altschul, S.F., Gish, W., Miller, W., Myers, E.W. and Lipman, D.J. (1990) Basic local alignment search tool. *J. Mol. Biol.* **215**, 403–410.
- Boratyn, G.M., Camacho, C., Cooper, P.S. *et al.* (2013) BLAST: a more efficient report with usability improvements. *Nucleic Acids Res.* **41**, W29–33.
- Bustin, S.A. (2000) Absolute quantification of mRNA using real-time reverse transcription polymerase chain reaction assays. *J. Mol. Endocrinol.* **25**, 169–193.
- Chakravarthy, A., Khan, L., Bensler, N.P., Bose, P. and De Carvalho, D.D. (2018) TGF-beta-associated extracellular matrix genes link cancer-associated fibroblasts to immune evasion and immunotherapy failure. *Nat. Commun.* **9**, 4692.
- Edwards, K., Johnstone, C. and Thompson, C. (1991) A simple and rapid method for the preparation of plant genomic DNA for PCR analysis. *Nucleic Acids Res.* **19**, 1349.
- Ender, F., Godl, K., Wenzl, S. and Sumper, M. (2002) Evidence for autocatalytic cross-linking of hydroxyproline-rich glycoproteins during extracellular matrix assembly in *Volvox*. *Plant Cell*, **14**, 1147–1160.
- Ender, F., Hallmann, A., Amon, P. and Sumper, M. (1999) Response to the sexual pheromone and wounding in the green alga *Volvox*: induction of an extracellular glycoprotein consisting almost exclusively of hydroxyproline. *J. Biol. Chem.* **274**, 35023–35028.
- Ertl, H., Mengele, R., Wenzl, S., Engel, J. and Sumper, M. (1989) The extracellular matrix of *Volvox carteri*: molecular structure of the cellular compartment. *J. Cell Biol.* **109**, 3493–3501.
- Fukada, K., Inoue, T. and Shiraishi, H. (2006) A posttranscriptionally regulated protease, VheA, is involved in the liberation of juveniles from parental spheroids in *Volvox carteri*. *Plant Cell*, **18**, 2554–2566.
- Godl, K., Hallmann, A., Rappel, A. and Sumper, M. (1995) Pherophorins: a family of extracellular matrix glycoproteins from *Volvox* structurally related to the sex-inducing pheromone. *Planta*, **196**, 781–787.
- Godl, K., Hallmann, A., Wenzl, S. and Sumper, M. (1997) Differential targeting of closely related ECM glycoproteins: the pherophorin family from *Volvox*. *EMBO J.* **16**, 25–34.
- Goodstein, D.M., Shu, S., Howson, R. *et al.* (2012) Phytozome: a comparative platform for green plant genomics. *Nucleic Acids Res.* **40**, D1178–1186.
- Gruber, H., Kirzinger, S.H. and Schmitt, R. (1996) Expression of the *Volvox* gene encoding nitrate reductase: mutation-dependent activation of cryptic splice sites and intron-enhanced gene expression from a cDNA. *Plant Mol. Biol.* **31**, 1–12.
- Hallmann, A. (2003) Extracellular matrix and sex-inducing pheromone in *Volvox*. *Int. Rev. Cytol.* **227**, 131–182.
- Hallmann, A. (2006) The pherophorins: common, versatile building blocks in the evolution of extracellular matrix architecture in Volvocales. *Plant J.* **45**, 292–307.

- Hallmann, A. (2011) Evolution of reproductive development in the volvocine algae. *Sex. Plant Reprod.* **24**, 97–112.
- Hallmann, A. and Kirk, D.L. (2000) The developmentally regulated ECM glycoprotein ISG plays an essential role in organizing the ECM and orienting the cells of *Volvox*. *J. Cell Sci.* **113**, 4605–4617.
- Hallmann, A. and Wodniok, S. (2006) Swapped green algal promoters: *aphVIII*-based gene constructs with *Chlamydomonas* flanking sequences work as dominant selectable markers in *Volvox* and vice versa. *Plant Cell Rep.* **25**, 582–591.
- Harris, E.H., Stern, D.B. and Witman, G.B. (2009) *The Chlamydomonas* Sourcebook, 2nd edn. San Diego, CA: Academic Press.
- Higuchi, R., Krummel, B. and Saiki, R.K. (1988) A general method of *in vitro* preparation and specific mutagenesis of DNA fragments: study of protein and DNA interactions. *Nucleic Acids Res.* **16**, 7351–7367.
- Holst, O., Christoffel, V., Fründ, R., Moll, H. and Sumper, M. (1989) A phosphodiester bridge between two arabinose residues as a structural element of an extracellular glycoprotein of *Volvox carteri*. *Eur. J. Biochem.* **181**, 345–350.
- Jean, C., Gravelle, P., Fournie, J.J. and Laurent, G. (2011) Influence of stress on extracellular matrix and integrin biology. *Oncogene*, **30**, 2697–2706.
- Johnson, M., Zaretskaya, I., Raytselis, Y., Merezuk, Y., McGinnis, S. and Madden, T.L. (2008) NCBI BLAST: a better web interface. *Nucleic Acids Res.* **36**, W5–9.
- Kianianmomeni, A. and Hallmann, A. (2013) Validation of reference genes for quantitative gene expression studies in *Volvox carteri* using real-time RT-PCR. *Mol. Biol. Rep.* **40**, 6691–6699.
- Kianianmomeni, A., Nematollahi, G. and Hallmann, A. (2008) A gender-specific retinoblastoma-related protein in *Volvox carteri* implies a role for the retinoblastoma protein family in sexual development. *Plant Cell*, **20**, 2399–2419.
- Kianianmomeni, A., Ong, C.S., Rättsch, G. and Hallmann, A. (2014) Genome-wide analysis of alternative splicing in *Volvox carteri*. *BMC Genom.* **15**, 1117.
- Kirk, D.L. (1998) *Volvox*: molecular-genetic origins of multicellularity and cellular differentiation. Cambridge: Cambridge University Press.
- Kirk, D.L. (2001) Germ-soma differentiation in *Volvox*. *Dev. Biol.* **238**, 213–223.
- Kirk, D.L. (2003) Seeking the ultimate and proximate causes of *Volvox* multicellularity and cellular differentiation. *Integr. Comp. Biol.* **43**, 247–253.
- Kirk, D.L. (2005) A twelve-step program for evolving multicellularity and a division of labor. *BioEssays*, **27**, 299–310.
- Kirk, D.L., Birchem, R. and King, N. (1986) The extracellular matrix of *Volvox*: a comparative study and proposed system of nomenclature. *J. Cell Sci.* **80**, 207–231.
- Kirk, D.L. and Kirk, M.M. (1986) Heat shock elicits production of sexual inducer in *Volvox*. *Science*, **231**, 51–54.
- Kirk, M.M. and Kirk, D.L. (2004) Exploring germ-soma differentiation in *Volvox*. *J. Biosci.* **29**, 143–152.
- Klein, B., Wibberg, D. and Hallmann, A. (2017) Whole transcriptome RNA-Seq analysis reveals extensive cell type-specific compartmentalization in *Volvox carteri*. *BMC Biol.* **15**, 111.
- Kremers, G.J., Goedhart, J., van Munster, E.B. and Gadella, T.W. Jr (2006) Cyan and yellow super fluorescent proteins with improved brightness, protein folding, and FRET Förster radius. *Biochemistry*, **45**, 6570–6580.
- Lauersen, K.J., Kruse, O. and Mussnug, J.H. (2015) Targeted expression of nuclear transgenes in *Chlamydomonas reinhardtii* with a versatile, modular vector toolkit. *Appl. Microbiol. Biotechnol.* **99**, 3491–3503.
- Lerche, K. and Hallmann, A. (2009) Stable nuclear transformation of *Gonium pectorale*. *BMC Biotechnol.* **9**, 64.
- Lerche, K. and Hallmann, A. (2013) Stable nuclear transformation of *Eudorina elegans*. *BMC Biotechnol.* **13**, 11.
- Lerche, K. and Hallmann, A. (2014) Stable nuclear transformation of *Pandorina morum*. *BMC Biotechnol.* **14**, 65.
- Lu, P., Takai, K., Weaver, V.M. and Werb, Z. (2011) Extracellular matrix degradation and remodeling in development and disease. *Cold Spring Harb Perspect Biol.* **3**.
- Matsuda, Y., Koseki, M., Shimada, T. and Saito, T. (1995) Purification and characterization of a vegetative lytic enzyme responsible for liberation of daughter cells during the proliferation of *Chlamydomonas reinhardtii*. *Plant Cell Physiol.* **36**, 681–689.
- Matusiewicz, M. (2011) Extracellular matrix remodeling. In *Encyclopedia of Cancer*, (ed. M. Schwab), pp. Berlin, Heidelberg: Springer.
- Merchant, S.S., Prochnik, S.E., Vallon, O. et al. (2007) The *Chlamydomonas* genome reveals the evolution of key animal and plant functions. *Science*, **318**, 245–250.
- Michod, R.E., Viostat, Y., Solari, C.A., Hurand, M. and Nedelcu, A.M. (2006) Life-history evolution and the origin of multicellularity. *J. Theor. Biol.* **239**, 257–272.
- Miller, D.H., Lampport, D.T.A. and Miller, M. (1972) Hydroxyproline heterooligosaccharides in *Chlamydomonas*. *Science*, **176**, 918–920.
- Mohan, V., Das, A. and Sagi, I. (2020) Emerging roles of ECM remodeling processes in cancer. *Semin. Cancer Biol.* **62**, 192–200.
- Nedelcu, A.M., Marcu, O. and Michod, R.E. (2004) Sex as a response to oxidative stress: a twofold increase in cellular reactive oxygen species activates sex genes. *Proc. R. Soc. Lond., B. Biol. Sci.* **271**, 1591–1596.
- Nedelcu, Aurora M. and Michod, Richard E. (2003) Sex as a response to oxidative stress: the effect of antioxidants on sexual induction in a facultatively sexual lineage. *Proceedings of the Royal Society of London. Series B: Biological Sciences*, **270**(suppl\_2), 136–139.
- Nishimura, M., Nagashio, R., Sato, Y. and Hasegawa, T. (2017) Late Somatic Gene 2 disrupts parental spheroids cooperatively with *Volvox* hatching enzyme A in *Volvox*. *Planta*, **245**, 183–192.
- Nozaki, H. (2003) Origin and evolution of the genera *Pleodorina* and *Volvox* (Volvocales). *Biologia (Bratisl.)*, **58**, 425–431.
- Pfaffl, M.W. (2001) A new mathematical model for relative quantification in real-time RT-PCR. *Nucleic Acids Res.* **29**, e45.
- Prochnik, S.E., Umen, J., Nedelcu, A.M. et al. (2010) Genomic analysis of organismal complexity in the multicellular green alga *Volvox carteri*. *Science*, **329**, 223–226.
- Provasoli, L. and Pintner, I.J. (1959) Artificial media for fresh-water algae: problems and suggestions. In *The Ecology of Algae, a symposium held at the Pymatuning Laboratory of Field Biology on June 18 and 19, 1959*, (ed. C.A. Tryon and R.T. Hartman), pp. 84–96. Pittsburgh, PA: The Pymatuning Symposia in Ecology, Special Publication No. 2, University of Pittsburgh.
- Sambrook, J. and Russell, D.W. (2001) *Molecular cloning: A laboratory manual*, 3rd edn. Cold Spring Harbor, NY: Cold Spring Harbor Laboratory Press.
- Schiedmeier, B., Schmitt, R., Müller, W., Kirk, M.M., Gruber, H., Mages, W. and Kirk, D.L. (1994) Nuclear transformation of *Volvox carteri*. *Proc. Natl. Acad. Sci. USA*, **91**, 5080–5084.
- Schindelin, J., Arganda-Carreras, I., Frise, E. et al. (2012) Fiji: an open-source platform for biological-image analysis. *Nat Methods*, **9**, 676–682.
- Schmitt, R. (2003) Differentiation of germinal and somatic cells in *Volvox carteri*. *Curr. Opin. Microbiol.* **6**, 608–613.
- Showalter, A.M. and Basu, D. (2016) Extensin and arabinogalactan-protein biosynthesis: glycosyltransferases, research challenges, and biosensors. *Front Plant Sci.* **7**, 814.
- Sommer-Knudsen, J., Bacic, A. and Clarke, A.E. (1998) Hydroxyproline-rich plant glycoproteins. *Phytochemistry*, **47**, 483–497.
- Sonbol, H.S. (2018) Extracellular matrix remodeling in human disease. *J. Microsc. Ultrastruct.* **6**, 123–128.
- Starr, R.C. (1969) Structure, reproduction and differentiation in *Volvox carteri* f. *nagariensis* lyengar, strains HK 9 & 10. *Arch. Protistenkd.* **111**, 204–222.
- Starr, R.C. (1970) Control of differentiation in *Volvox*. *Dev. Biol. Suppl.* **4**, 59–100.
- Starr, R.C. and Jaenicke, L. (1974) Purification and characterization of the hormone initiating sexual morphogenesis in *Volvox carteri* f. *nagariensis* lyengar. *Proc. Natl. Acad. Sci. USA*, **71**, 1050–1054.
- Strenkert, D., Schmollinger, S., Gallaher, S.D. et al. (2019) Multiomics resolution of molecular events during a day in the life of *Chlamydomonas*. *Proc. Natl. Acad. Sci. USA*, **116**, 2374–2383.
- Sumper, M., Berg, E., Wenzl, S. and Godl, K. (1993) How a sex pheromone might act at a concentration below  $10^{-16}$  M. *EMBO J.* **12**, 831–836.
- Sumper, M. and Hallmann, A. (1998) Biochemistry of the extracellular matrix of *Volvox*. *Int. Rev. Cytol.* **180**, 51–85.
- Tian, Y., Gao, S., von der Heyde, E.L., Hallmann, A. and Nagel, G. (2018) Two-component cyclase opsins of green algae are ATP-dependent and light-inhibited guanylyl cyclases. *BMC Biol.* **16**, 144.

**Wenzl, S. and Sumper, M.** (1981) Sulfation of a cell surface glycoprotein correlates with the developmental program during embryogenesis of *Volvox carteri*. *Proc. Natl. Acad. Sci. USA*, **78**, 3716–3720.

**Wenzl, S. and Sumper, M.** (1982) The occurrence of different sulphated cell surface glycoproteins correlates with defined developmental events in *Volvox*. *FEBS Lett.* **143**, 311–315.